ACS Photonics

Article

pubs.acs.org/journal/apchd5

Electric and Magnetic Field Enhancement with Ultralow Heat Radiation Dielectric Nanoantennas: Considerations for Surface-Enhanced Spectroscopies

Pablo Albella,*[,†] Rodrigo Alcaraz de la Osa,[‡] Fernando Moreno,[‡] and Stefan A. Maier[†]

[†]Experimental Solid State Group, Department of Physics, Imperial College London, London, SW7 2AZ, U.K.

[‡]Grupo de Óptica, Departamento de Física Aplicada, Universidad de Cantabria, Avenida de los Castros s/n, 39005 Santander, Spain

ABSTRACT: Plasmonic structures are known to offer strong local enhancements of the electric field for interaction with molecules and materials in their vicinity. However, they inherently suffer from high losses and absorption, which can occur in both surface plasmon polaritons and localized plasmons in particles, on which we shall focus. An effect of those losses, and an aspect often neglected, is the local heating of the nanoparticle due to the absorption of incident radiation and the transduction into thermal energy. This increase in the nanoparticle temperature, and in turn in the surrounding medium, can directly disrupt the response of the system due to changes in the optical properties of the medium and nanoparticle itself. This is especially a problem in the spectroscopic analysis of matter, where the advantage of field enhancement due to the plasmonic effect can be obstructed (or hampered) by a local temperature increase affecting the pure electromagnetic response of the sample. Here we investigate the use of subwavelength structures made of high refractive index dielectrics with ultralow losses in the optical and near-IR regime, gallium phosphide (GaP) in this case, as a novel way to approach applications that require near- and far-field enhancement, such as surface-enhanced Raman spectroscopy, but with the peculiarity of not perturbing the response of the sample under evaluation due to local heating. In particular, we show a comparison of the near- and far-field enhancing performance of plasmonic dimers with the one obtained from similar structures made of GaP. This study opens new possibilities to overcome losses and heat generation issues associated with plasmonic nanostructures in a range of applications in nanophotonics and metamaterials.

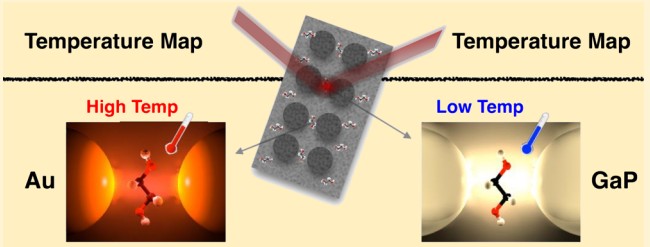

KEYWORDS: *SERS, SEIRA, sensing, plasmonics, low loss, field enhancement*

Plasmonics is a field that aims to exploit metallic nanostructures to control and manipulate light at the nanoscale and beyond the diffraction limit.[1,2] It is well known that metallic nanostructures possess the ability to show resonances in their optical response. These resonances, so-called surface plasmons, are given by the collective oscillation of the conduction electrons near the surface of the metal.[3] Numerous configurations[4,5] made of metallic nanostructures have been proposed and have been a subject of great interest and widely investigated for their potential use in technological and biological applications[6,7] in the wavelength range from 300 to 2000 nm. However, ohmic losses resulting from free-electron scattering in the metal is a major limitation for the performance of plasmonic structures, which in turn affect their spectral tunability.[8,9] Losses occur to surface plasmon polaritons at flat or rough interfaces as well as to localized plasmons in particles. In this work, we shall focus on the latter. Numerous attempts to design plasmonic materials with improved losses compared to metals have been recently performed by using unconventional plasmonic materials to control the complex permittivity of the structure, since this influences the resonant behavior and loss in plasmonic nanostructures.[10,11] Moreover, this unavoidable problem of losses in metallic structures is stimulating the study of subwavelength dielectric particles with high permittivity (such as silicon or germanium) as constitutive elements of new material designs and devices based on low-loss dielectric resonators.[12−16] These elements, apart from low losses, possess the ability to show not only electric resonances but also very intense magnetic ones.

Also, a lot of attention is recently being paid to dielectrics not only as an alternative to metal plasmonic antennas but also and more importantly as a source of magnetic response at optical frequencies.[17] In a recent work,[18] we showed how the optical response of dimers made of high refractive index dielectrics, silicon in particular, produces intense electric and magnetic fields outside the particles, which make them ideal candidates to enhance the emission of electric or magnetic emitters, thus becoming excellent dielectric optical nanoantennas.

An effect of losses in plasmonic metallic structures, and an aspect quite often neglected with respect to surface-enhanced Raman spectroscopy (SERS), is the local heating of the particle due to the absorption of incident radiation and the transduction

Received: February 21, 2014
Published: May 15, 2014

into thermal energy.[19−21] Theoretical and experimental studies have reported temperature increases ranging from 50 K under continuous excitation to as high as 1000 K using pulsed light sources.[22] This increase in the particle temperature, and in turn in the temperature of the surrounding medium, can directly influence the apparent SERS signal and has been attributed to several processes including thermal annealing, modified adsorption/desorption kinetics of surface molecules, and changes in the dielectric properties of the medium and the particle.[23] The physical implications and overall impact on the SERS signal of each of these processes may vary, but collectively are expected to influence the efficiency of both photophysical and chemical mechanisms. In Figure 1 we show

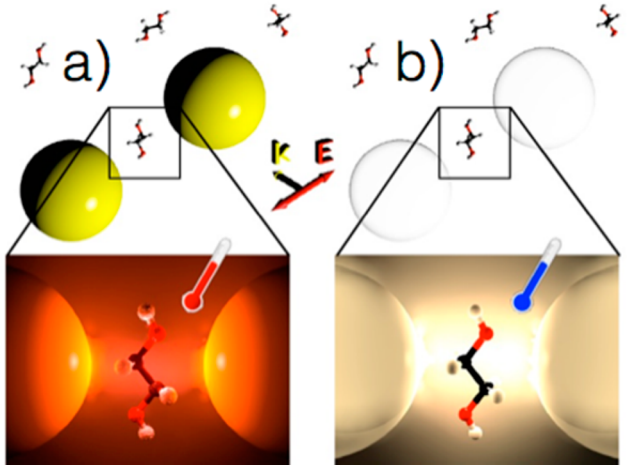

Figure 1. Artistic impression of a molecule located in the center of (a) a metallic dimer made of gold and (b) a dielectric dimer made of GaP.

an illustration of how heat generation may alter the response of the molecules that are the target of spectroscopic analysis. Figure 1a shows the action of a gold dimer working as a nanoantenna for SERS. Figure 1b shows the same SERS experiment but without altering the response of the molecules.

The aim of this work is to comprehensively investigate the use of subwavelength structures made of high refractive index dielectrics with ultralow losses in the optical and near-IR regime (gallium phosphide in this case) as a new way to approach surface-enhanced spectroscopies with the peculiarity of not perturbing the response of the target under evaluation. We will refer to these structures as ultralow heat nanoantennas.

METHODS

Theoretical Background. Nanoparticles (NPs) composed of various materials (such as Au, Ag, and semiconductors) can efficiently release heat under optical excitation. The heat generation process involves not only absorption of incident photons but also heat transfer from the NP to the surrounding matrix. The mechanism of heat release is very simple: the laser electric field strongly drives mobile carriers inside the material, and the energy gained by carriers turns into heat.

Then the heat diffuses away from the nanostructure and leads to an elevated temperature of the surrounding medium. Heat generation becomes especially strong in the case of metal NPs in the regime of plasmon resonance. In the case of semiconductor NPs, the heat generation rate is much weaker since heat dissipation occurs through an interband absorption process with the creation of a single mobile electron and hole (exciton). In the absence of phase transformations, the temperature distribution around optically stimulated NPs is described by the usual heat transfer equation:

$$\rho(r)\, c(r)\frac{\partial T(r,\, t)}{\partial t} = \nabla k(r)\, \nabla T(r,\, t) + Q_e(r,\, t) \tag{1}$$

where r and t are the coordinate and time, $T(r, t)$ is the local temperature, and the material parameters $\rho(r)$, $c(r)$, and $k(r)$ are the mass density, specific heat, and thermal conductivity, respectively. The solution of eq 1 has a transient state, and after a characteristic time, it reaches its steady state.[12,20−22] Thermal processes in metals are fast, which means that a steady state is rapidly reached (∼0.1 μs) for typical incident powers and metal NP dimensions, similar to those used in nanomedicine.[24,25] The function $Q_e(r, t)$ represents an energy (heat) source coming from light dissipation (electromagnetic losses) in NPs:

$$Q_e(r,\, t) = Q_{rh}(r,\, t) + Q_{ml}(r,\, t) \tag{2}$$

where the resistive losses are

$$Q_{rh}(r,\, t) = \langle j(r,\, t)\cdot E(r,\, t)_t \rangle = \frac{1}{2}\varepsilon_0\varepsilon_i\omega\, |E(r)|^2 \tag{3}$$

with $j(r, t)$ being the current density, $E(r, t)$ the stimulating electric field in the system, ε_0 the vacuum electric permittivity, ε_i the complex imaginary part of the relative electric permittivity of the material, and ω the angular frequency. Note that the 1/2 factor appears after time-averaging.

The magnetic losses $Q_{ml}(r, t)$ are given by

$$Q_{ml}(r,\, t) = \langle i\omega B(r,\, t)\cdot H(r,\, t)\rangle_t \tag{4}$$

where $B(r, t)$ and $H(r, t)$ are the magnetic flux density and the magnetic field intensity, respectively. In order to obtain the electromagnetic losses $Q_e(r, t)$, a system of Maxwell's equations including appropriate boundary conditions must be written, which in the case of an ensemble of NPs, such as a dimer, should be solved numerically. In our case, the whole process of light absorption and subsequent heat transfer between the nanostructure and the surrounding medium has been modeled by means of finite-element simulations. For easy implementation and reliability of the solution, we have chosen Comsol Multiphysics 4.3a (Comsol Inc., Burlington, MA, USA), which provides state-of-the-art routines to solve partial differential equations. In our simulations, we have assumed the electromagnetic losses from the electromagnetic waves in the NPs as the only heat source. We furthermore made the adiabatic assumption; that is, the electromagnetic cycle time (∼femtoseconds) is short compared to the thermal time scale (∼nanoseconds). In order to take into account heat dissipation in our simulation region, we used a heat flux node across the outer boundaries, defined by the equation

$$q_0 = h(T_{ext} - T) \tag{5}$$

where h is the heat transfer coefficient, dependent on the geometry and the ambient flow conditions, T_{ext} is the external temperature (assumed to be the same as the initial temperature of the system), and T is the temperature of the system. The heat transfer coefficient h can often be estimated by dividing the thermal conductivity of the convection fluid by a length scale.[23]

System Description. We have performed finite-element simulations on sphere and disk dimers made of gold (Au) and gallium phosphide (GaP) in the visible (vis, 450−900 nm)

dx.doi.org/10.1021/ph500060s | ACS Photonics 2014, 1, 524−529

range of the electromagnetic spectrum. All dielectric constants were taken from Palik.[26] In all cases, the dimers were illuminated under normal incidence with the electric field polarized along the line connecting the dimer. The incident power density was 1 mW/μm^2 in all cases, a typical value used in many applications.[27−29] If not stated otherwise, the dimers were embedded in air, with a gap equal to 10 nm. We chose appropriate sizes in order to have both Au and GaP resonances at the (approximately) same spectral position, although all results shown in this work are general and do not depend on the particular sizes chosen here.

Regarding the finite-element simulations, we used an approximated model based on a spherical simulation region of radius larger than a wavelength, together with a mesh fine enough as to allow convergence of the results. Most of these results have been obtained following the procedures previously outlined.[12,20−22]

RESULTS AND DISCUSSION

From a spectroscopic point of view (such as SERS or SEIRA), only the molecule−antenna near-field interaction and the enhancement of the molecule−antenna far-field radiation play an important role.[30] Thus, we have divided our results in far- and near-field, showing spectral cross sections in one case and spectral near-field enhancements and temperature increases in the other.

Far-Field. Figure 2 shows the absorption (σ_{abs}) and scattering (σ_{sca}) cross sections in the vis range for the case of (a) a Au sphere dimer of radius 50 nm and a GaP sphere dimer of radius 100 nm and (b) a Au disk dimer of radius 50 nm and height 37.5 nm and a GaP disk dimer of radius 100 nm and height 75 nm.

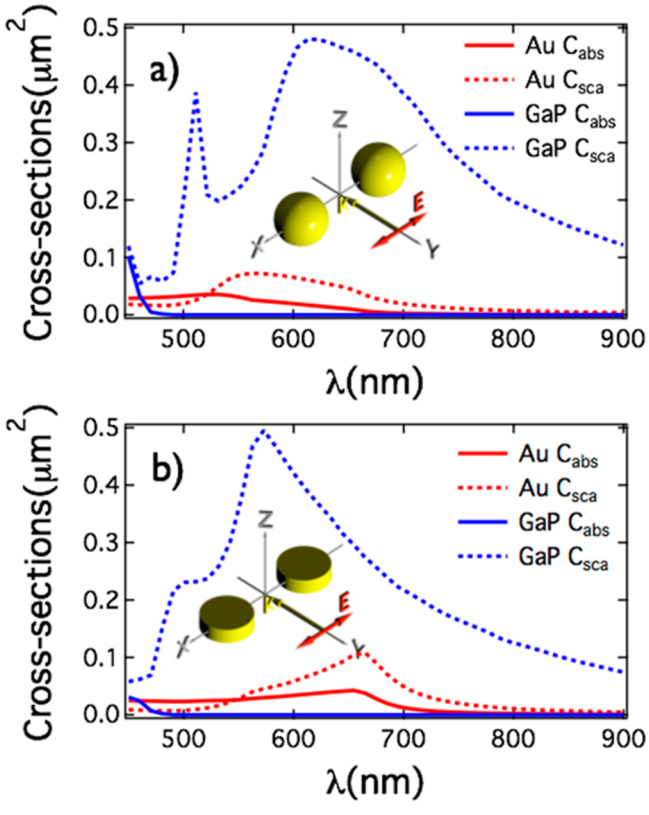

Figure 2. Absorption (σ_{abs}) and scattering (σ_{sca}) cross sections in the vis range for the case of (a) a Au sphere dimer of radius 50 nm and a GaP sphere dimer of radius 100 nm and (b) a Au disk dimer of radius 50 nm and height 37.5 nm and a GaP disk dimer of radius 100 nm and height 75 nm.

As shown and discussed in a previous work,[18] when two of these dielectric spheres are coupled together at close proximity, the electric and magnetic resonances interact, distorting and producing new spectral features. We observe that both the magnetic and the electric resonances are shifted in wavelength (the magnetic resonance to the blue and the electric resonance to the red). The broadening and the larger scattering cross section value of the peak around $\lambda \simeq 610$ nm is due to the overlap of both the electric and the magnetic dipolar modes. The sharp resonance around 500 nm comes from higher-order modes (more precisely, the magnetic quadrupolar mode). Although the original work was done in the near-infrared regime,[18] the same behavior can be observed in the visible range if the size parameter is adequately adapted.

Additionally, it can be seen that the GaP scattering cross section is as much as 5 times larger than that of Au for both spheres and disks. This makes GaP a very good competitor versus metals in terms of far-field enhancing performance. The GaP absorption cross section vanishes from 500 nm on. In this regime, within the transparent region of GaP (λ > 500 nm), particles made of this material can be treated as non-Rayleigh dipolar particles, as its index of refraction is real and large enough to exhibit electric and magnetic resonances.[9,31] For the case of gold, however, the absorption cross section is reasonably larger than that of GaP in most of the vis range. As we will see in Figure 5, this has a direct implication in the heat radiation exhibited by those structures, showing GaP as a clear candidate for applications where low heat radiation is required.

Near-Field. Figure 3 shows the electric field enhancement and the temperature difference (with respect to the initial temperature) in the center of the gap for sphere and disk dimers, for both Au and GaP in the vis range (the geometrical sizes are the same as in Figure 2). Unlike in the case of the far-field scattering cross section shown in Figure 2, the Au dimers offer a (as much as twice) better near electric field enhancement as compared with GaP. The near-field response of GaP is remarkably broadband though.

The temperature difference, however, shows a drastic contrast between Au and GaP, with temperature increases over 600 K in both sphere and disk Au dimers embedded in air. Going back to eq 3, it can be seen that the resistive losses partly depend on the complex imaginary part of the relative electric permittivity of the material ε_i. For the case of GaP, $\varepsilon_i = 0$ for most of the vis range (from 500 nm on), thus producing no resistive losses at all (no heat transfer) and therefore no temperature increase in the center of the gap (embedding medium).

Figure 4 shows the resistive losses for Au and GaP sphere dimers calculated at the absorption resonance of Au (taken from Figure 2, with the same geometrical sizes). As can be seen for the case of Au, the resistive losses are concentrated at the surface of the spheres, being zero in the surroundings (in accordance to eq 3, as the imaginary part of the air electric permittivity is zero). Equation 1 allows us to propagate the resistive losses (generated heat) to the embedding medium and obtain the temperature rise in the center of the gap. The GaP dimer shows no resistive losses at all, as specified by eq 3, given that the imaginary part of the electric permittivity of GaP is zero for λ > 500 nm. It is important to note that, for any

dx.doi.org/10.1021/ph500060s | ACS Photonics 2014, 1, 524−529

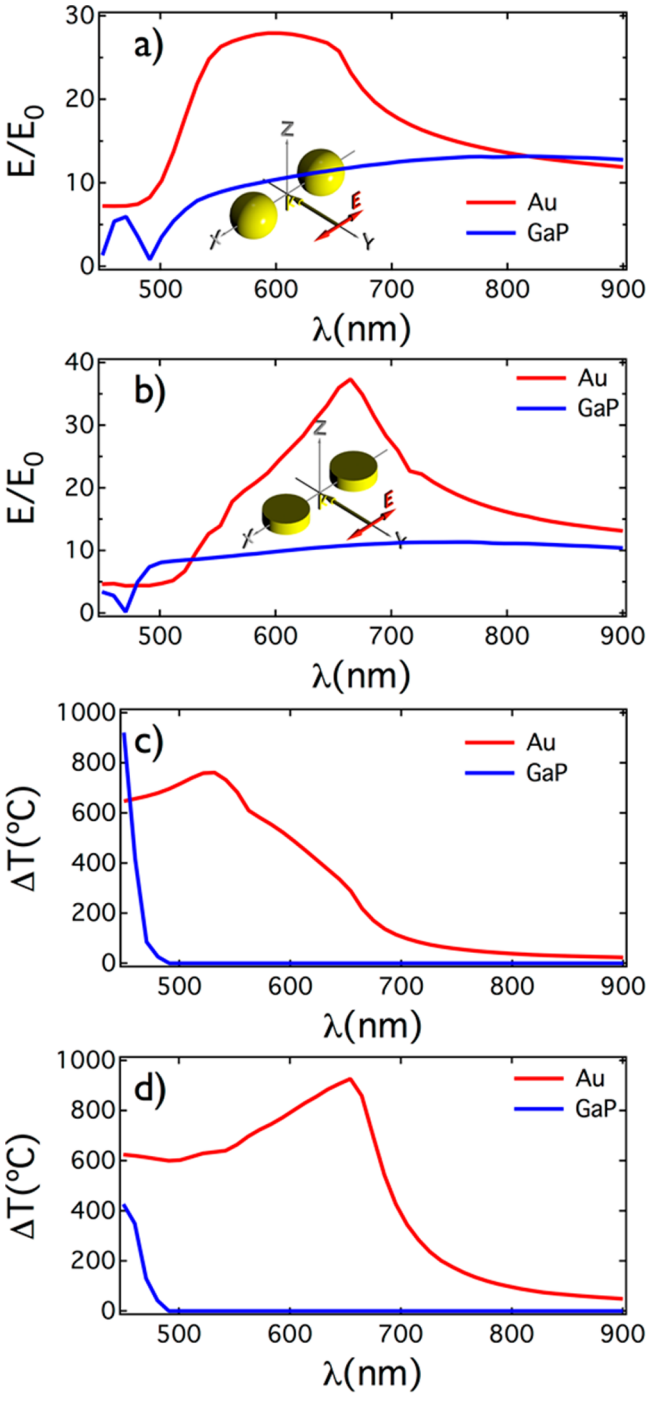

Figure 3. Electric field enhancement (a and b) and temperature difference (c and d) in the center of the gap for (a and c) a sphere dimer and (b and d) a disk dimer, for both Au and GaP in the vis range. The geometrical sizes are the same as in Figure 2

practical realization, metal impurities will cause the imaginary part of the electric permittivity (and therefore losses) to be nonzero, but still very low.

In Figure 5 we show the temperature difference in the center of the gap of a sphere dimer calculated at the absorption resonance of Au (taken from Figure 2, with the same geometrical sizes) as a function of the incident power density, for both Au and GaP in the vis range. It can be seen that the temperature rise in the center of the dimer gap strongly depends on the incident power density. The GaP case once again presents no temperature difference at all regardless of the incident power density.

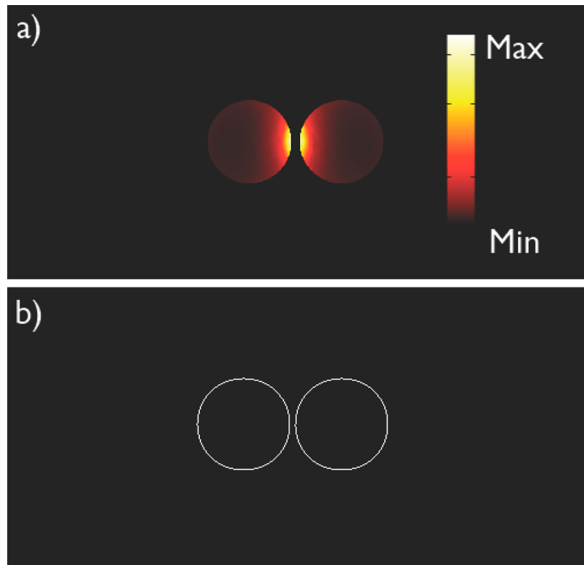

Figure 4. Resistive losses for (a) Au and (b) GaP sphere dimer calculated at the absorption resonance of Au (taken from Figure 2, with the same geometrical sizes).

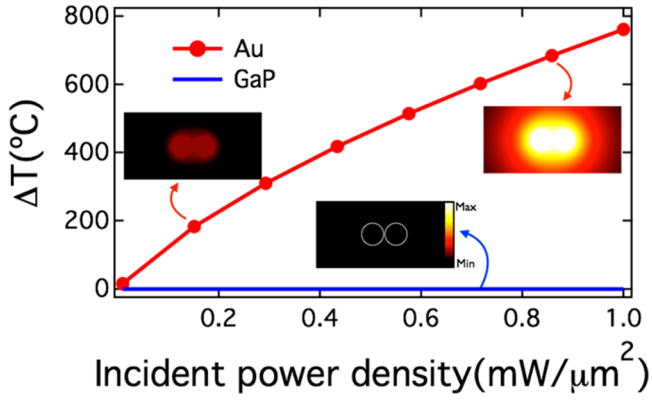

Figure 5. Temperature difference in the center of the dimer calculated at the absorption resonance of Au (taken from Figure 2, with the same geometrical sizes) as a function of the incident power density, for both Au and GaP in the vis range. The insets show the temperature distribution around the sphere dimer for selected incident power densities.

Notice that the dependence of the temperature increase on the incident power density is not perfectly linear, due to the interaction of the particles and the field localization in the gap.

In order to clearly illustrate one of the possible influences that a temperature rise may have in the plasmonic response of nanostructures in a real situation, we have explicitly considered the case of a single gold sphere embedded in a surrounding medium with a temperature-dependent refractive index. This system tries to mirror the effect of a molecular sample embedded in an aqueous medium such as those typically used in spectroscopy experiments, such as SERS, SEIRA, or biological sensing.[32] Regarding the temperature-dependent refractive index n_{sm}, we have relied on the temperature dependence of the refractive index of air (in the ideal gas limit), but adapted to the case of an aqueous ambient medium:

dx.doi.org/10.1021/ph500060s | ACS Photonics 2014, 1, 524−529

$$n_{sm}(\Delta T) = 1 + \frac{33}{100 + \Delta T} \quad (6)$$

Figure 6a shows the temperature-dependent refractive index of the surrounding medium as given by eq 6. Taking Figure 3c into account, we may connect the temperature difference with the incident wavelength and therefore calculate the wavelength dependence of the surrounding medium's refractive index, which is shown in Figure 6b. The reference case $\Delta T = 0$ °C (shown by the dashed red line) corresponds to an aqueous ambient medium ($n_{sm} = 1.33$).

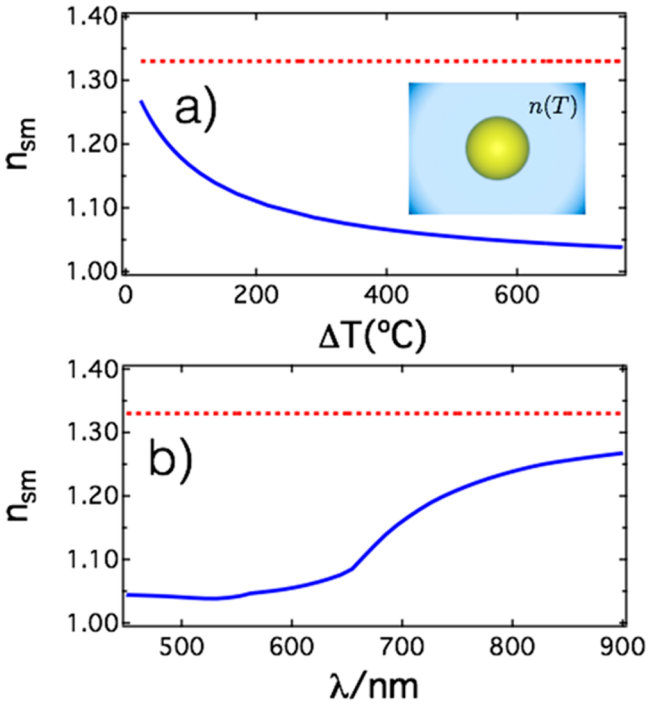

Figure 6. (a) Temperature and (b) wavelength dependence of the refractive index of the surrounding medium n_{sm}, as given by eq 6 and the wavelength-dependent temperature difference shown in Figure 3c. The dashed red line corresponds to the reference case $\Delta T = 0$ °C.

As expected, the biggest departure from the $\Delta T = 0$ °C case occurs at the resonance position (around $\lambda = 550$ nm), where the temperature difference is largest and therefore the deviation of the refractive index from the reference case is maximum too. Notice that, as shown in Figure 6, the refractive index of the surrounding medium decreases as we increase the temperature difference. Thus, a blue-shift of the resonance peak is expected, corroborated by Figure 7, which shows the spectral extinction efficiency for an isolated sphere made of gold of radius $R = 50$ nm embedded in a surrounding medium with a temperature-dependent refractive index n_{sm} given by eq 6. The wavelength-dependent temperature difference has been taken from Figure 3c. The dashed red line corresponds to the reference case $\Delta T = 0$ °C.

As expected, the resonance peak blue-shifts with respect to the reference case ($\Delta T = 0$ °C) when embedding the gold nanosphere in the surrounding medium with a temperature-dependent refractive index. This is because the surrounding medium's refractive index decreases as we increase the temperature difference (as shown in Figure 6). In a typical SERS experiment, if we were to accurately excite the plasmonic resonance of such a gold nanoparticle embedded in the aforementioned medium, we should take into account the blue-shift associated with the temperature difference.

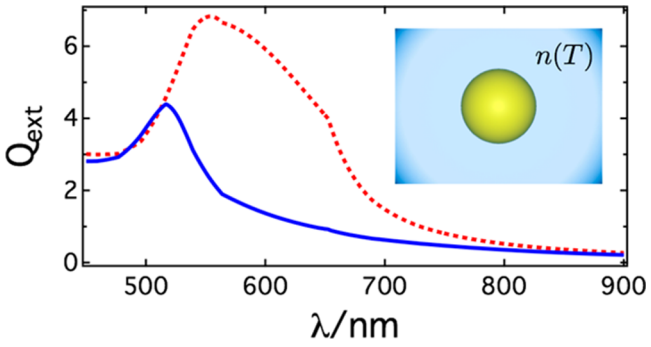

Figure 7. Spectral extinction efficiency for an isolated sphere made of gold of radius $R = 50$ nm embedded in a surrounding medium with a temperature-dependent refractive index given by eq 6. The wavelength-dependent temperature difference has been taken from Figure 3c. The dashed red line corresponds to the reference case $\Delta T = 0$ °C.

CONCLUSIONS

The effect of the losses, inherent to plasmonic structures and leading to the local heating of the particle due to the absorption of incident radiation, is an aspect often neglected despite the fact that it is of critical importance when seeking to perform unperturbed molecular spectroscopy. A full electrodynamical study was performed, comparing the optical response of subwavelength metallic (Au) and dielectric (GaP) dimers acting as nanoantennas in the near- and far-field region, with the aim of finding a material that can overcome this plasmonic losses problem but providing enough far- and near-field enhancement, which is a prerequisite for surface-enhanced spectroscopies. We have numerically demonstrated that even though the near-field-enhancing capability of GaP nanoparticles is comparatively less intense than that provided by metallic nanoparticles, the stronger far-field enhancement together with the absence of losses makes it a promising alternative candidate to perform surface-enhanced spectroscopies. Also, these ultra-low-heat antennas open the path to extend these spectroscopies to samples that may exhibit not only electric but also magnetic optical response and, more importantly, without external heat perturbation that may disturb the sample response.

AUTHOR INFORMATION

Corresponding Author

*E-mail: p.albella@imperial.ac.uk.

Notes

The authors declare no competing financial interest.

ACKNOWLEDGMENTS

This work was supported by the Leverhulme Trust and the EPSRC Active Plasmonics Programme.

REFERENCES

(1) Schuller, J. A.; Barnard, E. S.; Cai, W.; Jun, Y. C.; White, J. S.; Brongersma, M. L. Plasmonics for extreme light concentration and manipulation. *Nat. Mater.* **2010**, *9* (3), 193−204.

(2) Stockman, M. Nanoplasmonics: past, present, and glimpse into future. *Opt. Express* **2011**, *19*, 22029−22106.

(3) Maier, S. A. *Plasmonics−Fundamentals and Applications*; Springer: New York, 2007.

(4) Maier, S. A.; Atwater, H. A. Plasmonics: localization and guiding of electromagnetic energy in metal/dielectric structures. *J. Appl. Phys.* **2005**, *98*, 011101.
(5) Novotny, L.; van Hulst, N. Antennas for light. *Nat. Photonics* **2011**, *5*, 83−90.
(6) Stockman, M. I. Nanoplasmonics: the physics behind the applications. *Phys. Today* **2011**, *64*, 39.
(7) Anker, J. N.; Hall, W. P.; Lyandres, O.; Shah, N. C.; Zhao, J.; Van Duyne, R. P. Biosensing with plasmonic nanosensors. *Nat. Mater.* **2008**, *7* (6), 442−53.
(8) Moreno, F.; Albella, P.; Nieto-Vesperinas, M. Analysis of the spectral behavior of localized plasmon resonances in the near- and far-field regimes. *Langmuir* **2013**, *29* (22), 6715−21.
(9) Geffrin, J. M.; García-Cámara, B.; Gómez-Medina, R.; Albella, P.; Froufe-Pérez, L. S.; Eyraud, C.; Litman, A.; Vaillon, R.; Gonzalez, F.; Nieto-Vesperinas, M.; Sáenz, J. J.; Moreno, F. Magnetic and electric coherence in forward- and back-scattered electromagnetic waves by a single dielectric subwavelength sphere. *Nat. Commun.* **2012**, *3*, 1171.
(10) Popa, B. I.; Cummer, S. A. Compact dielectric particles as a building block for low-loss magnetic metamaterials. *Phys. Rev. Lett.* **2008**, *100*, 207401.
(11) Valentine, J.; Zhang, S.; Zentgraf, T.; Ulin-Avila, E.; Genov, D. A.; Bartal, G.; Zhang, X. Three-dimensional optical metamaterial with a negative refractive index. *Nature* **2008**, *455*, 376−379.
(12) Baffou, G.; Quidant, R.; Girard, C. Heat generation in plasmonic nanostructures: influence of morphology. *Appl. Phys. Lett.* **2009**, *94*, 153109.
(13) Lapotko, D. O. Therapy with gold nanoparticles and lasers: what really kills the cells? *Nanomedicine* **2009**, *4*, 253.
(14) Zou, L.; Withayachumnankul, W.; Shah, C. M.; Mitchell, A.; Bhaskaran, M.; Sriram, S.; Fumeaux, C. Dielectric resonator nano-antennas at visible frequencies. *Opt. Express* **2013**, *21*, 1344−1352.
(15) Staude, I.; Miroshnichenko, A. E.; Decker, M.; Fofang, N. T.; Liu, S.; Gonzales, E.; Dominguez, J.; Luk, T. S.; Neshev, D. N.; Brener, I.; Kivshar, Y. Tailoring directional scattering through magnetic and electric resonances in subwavelength silicon nanodisks. *ACS Nano* **2013**, *7*, 7824−7832.
(16) Yang, Y.; Wang, W.; Moitra, P.; Kravchenko, I. I.; Briggs, D. P.; Valentine, J. Dielectric meta-reflectarray for broadband linear polarization conversion and optical vortex generation. *Nano Lett.* **2014**, *14*, 1394−1399.
(17) Ginn, J. C.; Brener, I.; Peters, D. W.; Wendt, J. R.; Stevens, J. O.; Hines, P. F.; Basilio, L. I.; Warne, L. K.; Ihlefeld, J. F.; Clem, P. G.; Sinclair, M. B. Realizing optical magnetism from dielectric metamaterials. *Phys. Rev. Lett.* **2012**, *108*, 097402.
(18) Albella, P.; Poyli, M. A.; Schmidt, M. K.; Maier, S. A.; Moreno, F.; Sáenz, J. J.; Aizpurua, J. Low-loss electric and magnetic field-enhanced spectroscopy with subwavelength silicon dimers. *J. Phys. Chem. C* **2013**, *117*, 13573.
(19) Seol, Y.; Carpenter, A. E.; Perkins, T. T. Gold nanoparticles: enhanced optical trapping and sensitivity coupled with significant heating. *Opt. Lett.* **2006**, *31*, 2429.
(20) Govorov, A. O.; Zhang, W.; Skeini, T.; Richardson, H. H.; Lee, J.; Kotov, N. A. Gold nanoparticle ensembles as heaters and actuators: melting and collective plasmon resonances. *Nanoscale Res. Lett.* **2006**, *1*, 84.
(21) Baffou, G.; Quidant, R.; García de Abajo, F. J. Nanoscale control of optical heating in complex plasmonic systems. *ACS Nano* **2010**, *4*, 709.
(22) Govorov, A. O.; Richardson, H. H. Generating heat with metal nanoparticles. *Nano Today* **2007**, *2*, 30.
(23) King, M. D.; Khadka, S.; Craig, G. A.; Mason, M. D. The effect of local heating on the SERS efficiency of single optically trapped prismatic nanoparticles. *J. Phys. Chem. C* **2008**, *112*, 11751.
(24) Liu, X.; Lloyd, M. C.; Fedorenko, I. V.; Bapat, P.; Zhukov, T.; Huo, Q. Enhanced imaging and accelerated photothermalysis of A549 human lung cancer cells by gold nanospheres. *Nanomedicine* **2008**, *3*, 617.
(25) Hleb, E. Y.; Hafner, J. H.; Myers, J. N.; Hanna, E. Y.; Rostro, B. C.; Zhdanok, S. A.; Lapotko, D. O. LANTCET: elimination of solid tumor cells with photothermal bubbles generated around clusters of gold nanoparticles. *Nanomedicine* **2008**, *3*, 647.
(26) Palik, E. D. *Handbook of Optical Constants of Solids*; Academic Press: New York, 2007.
(27) Michalet, X.; Weiss, S. Single-molecule spectroscopy and microscopy. *C. R. Phys.* **2002**, *3*, 619.
(28) Kneipp, K.; Kneipp, H.; Abdali, S.; Berg, R. W.; Bohr, H. Single molecule Raman detection of enkephalin on silver colloidal particles. *J. Spectrosc.* **2004**, *18*, 433.
(29) Botta, R.; Upender, G.; Sathyavathi, R.; Rao, D. N.; Bansal, C. Silver nanoclusters films for single molecule detection using surface enhanced raman scattering (SERS). *Mater. Chem. Phys.* **2013**, *137*, 699.
(30) Alonso-González, P.; Albella, P.; Schnell, M.; Chen, J.; Huth, F.; García-Etxarri, A.; Casanova, F.; Golmar, F.; Arzubiaga, L.; Hueso, L. E.; Aizpurua, J.; Hillenbrand, R. Resolving the electromagnetic mechanism of surface-enhanced light scattering at single hot spots. *Nat. Commun.* **2012**, *3*, 684.
(31) García-Etxarri, A.; Gómez-Medina, R.; Froufe-Pérez, L. S.; López, C.; Chantada, L.; Scheffold, F.; Aizpurua, J.; Nieto-Vesperinas, M.; Sáenz, J. J. Strong magnetic response of submicron silicon particles in the infrared. *Opt. Express* **2011**, *19*, 4815.
(32) Willets, K. A.; Van Duyne, R. P. Localized surface plasmon resonance spectroscopy and sensing. *Annu. Rev. Phys. Chem.* **2007**, *58*, 267−297.